Highly Efficient Nonisolated Constant Output Current *LCC* Resonant Converter With Wide Input Voltage Range

Shirin Askari and Hosein Farzanehfard, *Member, IEEE*

***Abstract*—In this article, we propose a simple structure highly efficient low-element-count nonisolated constant output current resonant converter for wide input voltage range and high-efficient applications. The converter is developed by combining a basic buck–boost converter with a half-bridge *LCC* resonant converter to improve the adjustable voltage conversion ratio. In the proposed structure, most of the output power is fed directly, which reduces the conduction power losses and increases efficiency by the reduction of the processed power, and the switches and rectifier diodes' voltage stress is significantly decreased due to cascaded outputs structure. It operates at the resonant frequency to achieve a constant output current feature for applications, such as LED drivers and battery chargers, and the output current is regulated by the pulsewide modulation. The proposed converter can achieve zero-voltage switching operation for all switches and zero-current switching operation for all diodes over a wide range of the input voltage and load conditions. The proposed structure is analyzed in detail. To verify the proposed converter performance, a 21-W laboratory prototype is realized and tested for the wide input voltage range of 12–40 V to provide 350 mA output current. The proposed converter achieves a high peak efficiency of 98.15%.**

***Index Terms*—Constant output current resonant converter, high efficient, load independent, wide input voltage range, zero-voltage switching (ZVS).**

I. Introduction

IN SOME applications, such as LED drivers and battery chargers, a constant output current converter is required [1], [2], [3]. Some resonant converters provide an intrinsic constant output current when operated at the resonance frequency. In addition to this characteristic, operating at resonance frequency reduces the circulating loss and optimizes the converter size [4], [5]. The conventional pulse frequency modulation method is popular for controlling the resonant converters. However, the switching frequency needs to vary away from the resonant frequency and the constant output current characteristic is deteriorated, which results in high circulating energy and consequently lower efficiency [6]. Pulsewidth modulation (PWM) and phase-shifted modulation (PSM) PWM are employed to control the current or voltage conversion ratio of the constant-frequency resonant converters. However, regular PWM method suffers from narrow adjustment of the voltage gain where PSM PWM can achieve a wider voltage gain adjustment, but the circulating current of the converter increases [7], [8], [9], [10], [11], [12].

To modify the conventional resonant converters voltage gain, numerous fixed-frequency control schemes and topologies are proposed. Thus, the converter conversion ratio is changed in a wide range by adjusting the switches duty cycle. These control methods can be categorized as follows:

1) reconfigurable structures using some switches for alternating the topology between different operation [13], [14], [15], [16];
2) hybrid structures, which merges or combines basic PWM converters with conventional resonant converters [17], [18];
3) integrating reconfigurable and hybrid structures [19], [20].

In the resonant converter of Kim and Barbosa [13], two of the full-bridge rectifier diodes are replaced with two switches to create a dual rectifier and provide a wide voltage conversion ratio range by switching between half-bridge and full-bridge rectifier states. However, adding two switches in the secondary makes the control complicated. In [17], a buck–boost converter is combined with an *LLC* resonant converter to achieve a wide conversion ratio with PWM control scheme. However, the freewheeling mode causes considerable power loss. By merging a buck–boost and a hybrid mode series resonant converter, a triple-mode resonant converter is presented in [19]. The secondary bridgeless rectifier enables the converter to operate in three different modes of resonant boost, series resonant, and PWM series resonant buck, depending on the input voltage level. In each mode, the output voltage is regulated by the PWM control of the buck–boost main switches. Although this circuit provides a wide voltage gain range, but one of the main switches suffers from hard switching. In [20], a reconfigurable converter with three different configurations is provided by combining a buck–boost and a full-bridge series resonant converter. By switching from one configuration to another, depending on the input voltage level, a wide input voltage range is regulated. However, due to the operation away from the resonance frequency, the circulating loss is high, and the output voltage is load dependent. By Merging a flyback and a series resonant

Manuscript received 24 November 2022; revised 22 February 2023; accepted 22 May 2023. Date of publication 25 May 2023; date of current version 21 June 2023. Recommended for publication by Associate Editor G. Moschopoulos. *(Corresponding author: Hosein Farzanehfard.)*

The authors are with the Department of Electrical and Computer Engineering, Isfahan University of Technology, Isfahan 84156-83111, Iran (e-mail: s.askari@ec.iut.ac.ir; hosein@iut.ac.ir).

Color versions of one or more figures in this article are available at https://doi.org/10.1109/TPEL.2023.3280119.

Digital Object Identifier 10.1109/TPEL.2023.3280119

converter, the three-mode resonant converter in [18] is provided. It operates in three modes of low, medium, and high voltage gain by applying three different PWM modulations to achieve wide voltage gain. However, the flyback transformer leakage inductance is discharged in the switches while the capacitive turn-ON loss of switches is not eliminated. The converters proposed in [14], [15], and [16] suffer from a large number of elements. In [16], a resonant converter with two *LLC* resonant networks is presented, which operates in two separate modes of low gain and medium gain to provide a wide voltage gain range. In [15], a resonant converter with a dual-mode rectifier on the secondary is presented for wide voltage gain applications. A reconfigurable series resonant converter with quadruple-mode structure using a dual-bridge at the primary and a dual-rectifier on the secondary is proposed in [14]. Depending on the input and output voltage levels, the operating mode is selected.

In this article, a novel nonisolated constant output current resonant converter is proposed, which is formed by merging a buck–boost with an *LCC* resonant converter to regulate a wide input voltage range. Due to cascaded outputs structure, the converter efficiency and conduction losses are improved since a part of the output power processed directly and the switches and rectifier diodes voltage stress are reduced. The input voltage is regulated by applying a fixed-frequency control using the buck–boost switches duty cycle. Also, the *LCC* network provides the load-independent output current by operating at the resonant frequency (f_r), which provides another advantage of eliminating high circulating loss and efficiency degradation. Zero-voltage switching (ZVS) and zero-current switching (ZCS) operation are provided for all switches and diodes, respectively, due to employing *LCC* resonant network. It should be noted that such advantages are achieved by employing a simple structure.

The rest of this article is organized as follows. The operating principles of the proposed converter are introduced in Section II. The converter steady-state analysis is presented in Section III and the experimental results are discussed in Section IV. Finally, Section V concludes this article.

II. Proposed Converter Operation Principles

A. Topology Description

The proposed resonant converter presented in Fig. 1 is provided by combining a buck–boost and a half-bridge *LCC* resonant converter. The converter consists of *LCC* resonant network (C_{r1}, C_{r2}, and L_r), voltage-doubler rectifier (D_{o1} and D_{o2}), buck–boost elements (L_{BB} and C_{BB}), inverter switches (S_1 and S_2), and voltage-doubler output capacitor (C_o). The output voltage (V_o) is equal to the summation of input voltage source (V_{in}), the buck–boost output voltage (V_{CBB}), and the voltage-doubler output voltage (V_{o1}). As observed from Fig. 1, V_{in} and C_{BB} are connected in series with C_o to reduce the processed power and improve efficiency. This feature can be only achieved by using the buck–boost topology with the inverted output voltage. As a result, most of the power is directly transferred from V_{in} to the output without any processing. Therefore, the power processing and the conduction losses are minimized, which contributes to higher efficiency. In this structure, C_{BB} and C_o jointly and coordinately perform the task of regulating the output voltage, which results in a wide adjustment of the voltage gain. Another advantage provided by connecting V_{in}, C_{BB}, and C_o in series is reduction of the inverter switches and output rectifier diodes' voltage stress.

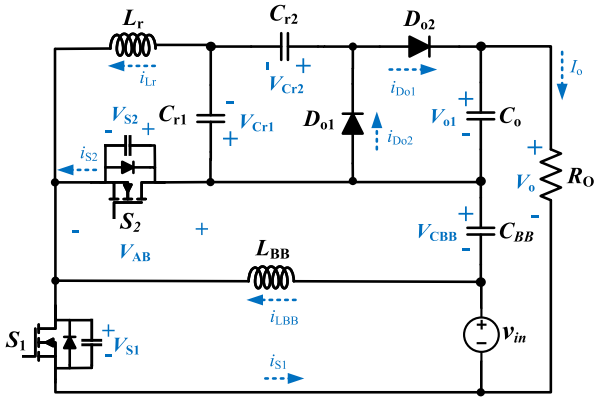

Fig. 1. Proposed resonant converter.

B. Operating Principles

The proposed converter key waveforms are shown in Fig. 2 where the gate signals S_1 and S_2 are complementary. The converter operation is divided into eight operating modes, and the equivalent circuit in each mode is shown in Fig. 3(a)–(h).

Mode 1 [t_0–t_1]: The first mode starts by turning S_1 ON under ZVS condition. In this mode, the diode D_{o1} is reverse biased and D_{o2} is conducting, which applies V_{o1} to *LCC* network output. Also, (V_{in}+V_{CBB}) is applied to *LCC* network input. The inductor L_{BB} is charged through V_{in} and the output power is fed through (V_{in}+V_{CBB}+V_{o1}). The *LCC* network elements are resonating and L_r is charging and resonant capacitors are discharging. At t_1, D_{o2} turns OFF and this mode ends.

Mode 2 [t_1–t_2]: During this mode, D_{o1} and D_{o2} do not conduct and C_{r2} does not participate in the resonance, so its voltage remains constant. C_{r1} and L_r are charging in a sinusoidal fashion through a resonance. At the end of this mode at t_2, D_{o1} start to conduct and *LCC* output is short circuited.

Mode 3 [t_2–t_3]: As D_{o1} starts conducting at the beginning of this mode, C_{r2} begins to participate in the resonance with other *LCC* resonant elements and charging, such as C_{r1}. This mode ends when S_1 is turned OFF at t_3.

Mode 4 [t_3–t_4]: When S_1 turns OFF, the summation of I_{LBB} and I_{Lr} starts charging and discharging S_1 and S_2 output capacitors, respectively. After S_2 output capacitor is discharged completely, its body diode starts conducting and then, S_2 can be turned ON under ZVS condition.

Mode 5 [t_4–t_5]: S_2 and D_{o1} conduct during this mode, and D_{o2} is reverse biased. Also, the *LCC* network output and input are short circuited and the inductor L_{BB} is discharged via V_{CBB}. The *LCC* network elements are resonating, which causes L_r to discharge and the resonant capacitors to charge. This mode ends

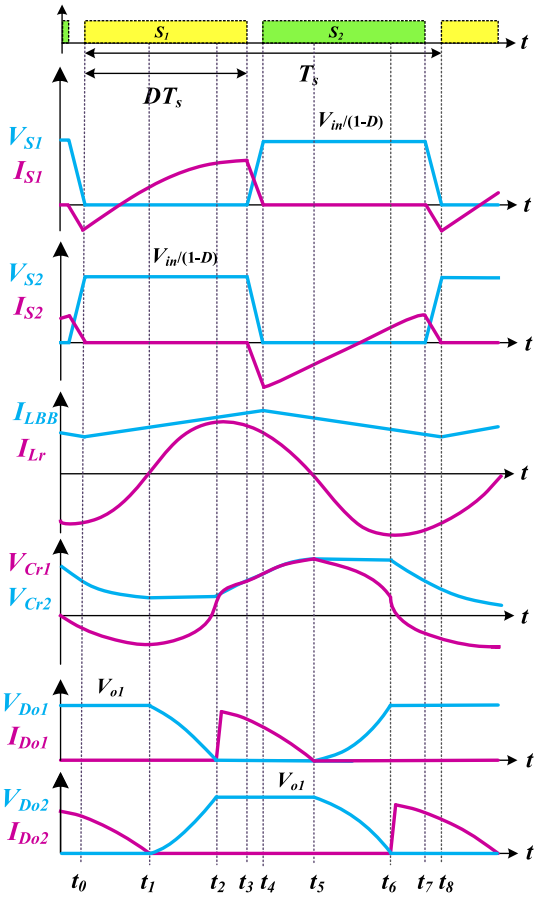

Fig. 2. Proposed resonant converter key waveforms.

when C_{r2} current reaches zero and D_{o1} turns OFF at t_5 under ZCS condition.

Mode 6 [t_5–t_6]: During this mode, the rectifying output diodes are in the OFF state. Also, the C_{r2} voltage stays constant while C_{r1} and L_r are discharging through a resonance. D_{o2} starts to conduct at the end of this mode at t_6, which applies V_{o1} to the *LCC* network output.

Mode 7 [t_6–t_7]: This mode begins when D_{o2} starts to conduct, and C_{r2} begins to participate in the resonant network. This mode ends when S_2 is turned OFF at t_7.

Mode 8 [t_7–t_8]: By turning S_2 OFF, the output capacitors of S_2 and S_1 start charging and discharging, respectively, by the current summation of I_{LBB} and I_{Lr}. After S_1 output capacitor is fully discharged, the S_1 body diode starts to conduct and S_1 can be turned ON under ZVS condition.

III. Proposed Converter Analysis

A. Voltage Gain

The proposed constant output current resonant converter analysis is carried out under steady-state condition with the assumption of ideal MOSFETs and diodes. Due to operating the converter at the resonant frequency, the fundamental harmonic approximation analysis can be carried out for theoretical analysis [4]. V_{CBB} is obtained as follows:

$$V_{CBB} = \frac{D}{1-D} V_{\text{in}} \tag{1}$$

where D is the S_1 duty cycle. The *LCC* resonant network ac equivalent circuit is shown in Fig. 4. V_{AB} is asymmetric square waveform voltage with (V_{in}+ V_{CBB}) amplitude applied to the resonant network input, and V_{AC} is the resonant network output voltage. The V_{AB} fundamental harmonic amplitude is obtained as follows:

$$V_{AB}^{F} = \frac{2V_{\text{in}}\sin(\pi D)}{\pi(1-D)}\cos(\omega_s t) \tag{2}$$

where $\omega_s = \omega_r = \frac{1}{\sqrt{L_r C_{r1}}}$. The *LCC* resonant network voltage and current gain are attained as follows:

$$M(j\omega_n) = \frac{V_{AC}}{V_{AB}} = \frac{jC_n\omega_n}{Q(1-{\omega_n}^2(1+C_n))+jC_n\omega_n(1-{\omega_n}^2)} \tag{3}$$

$$H(j\omega_n) = \frac{I_{AC}}{\frac{V_{AB}}{Z_0}} = \frac{jQC_n\omega_n}{Q(1-{\omega_n}^2(1+C_n))+jC_n\omega_n(1-{\omega_n}^2)} \tag{4}$$

where ω_n, C_n, Z_0, and Q are normalized frequency, resonant capacitors ratio, characteristic impedance, and quality factor, respectively, as defined in the following:

$$\omega_n = \frac{\omega_s}{\omega_r} = \frac{f_s}{f_r},\ C_n = \frac{C_{r2}}{C_{r1}},\ Z_0 = \sqrt{\frac{L_r}{C_{r1}}},\ Q = \frac{Z_0}{R_{ac}} \tag{5}$$

where R_{ac} is the *LCC* resonant network equivalent output resistance and are calculated as $R_{ac} = \frac{2R_{o1}}{\pi^2}$ where R_{o1} is the rectifier equivalent output resistance and is obtained as follows:

$$R_{o1} = \frac{P_o}{I_o^2} - \frac{V_{\text{in}}}{I_o(1-D)} \tag{6}$$

where P_o and I_o are the output power and current, respectively. The proposed converter output current is calculated as follows:

$$I_o(\omega_n = 1) = \frac{2V_{\text{in}}\sin(\pi D)}{\pi^2(1-D)Z_0}. \tag{7}$$

The magnitude plot of $H(j\omega_n)$ versus ω_n at different Q and C_n values is presented in Fig. 5(a) and (b), respectively. Also, the normalized output current $\frac{I_o}{(\frac{V_{\text{in}}}{Z_0})}$ for various duty cycles is shown in Fig. 5(c). As observed from Fig. 5(a) and (b), by operating at the resonant frequency, a load-independent output current characteristic can be achieved. Also, the excellent constant output current characteristic of the proposed converter can be seen in Fig. 5(c).

B. Switches and Diodes Voltage and Current Stress

The switches voltage stress $V_{S,\text{peak}}$ is limited to the summation of V_{CBB} and V_{in} while the switches current stress $I_{S,\text{peak}}$ is limited to the summation of I_{Lm} and I_{Lr} at t_3, as shown in the following:

$$V_{S,\text{peak}} = \frac{V_{\text{in}}}{1-D}\ ,\quad I_{S,\text{peak}} = I_{Lr}(t_3) + I_{LBB} \tag{8}$$

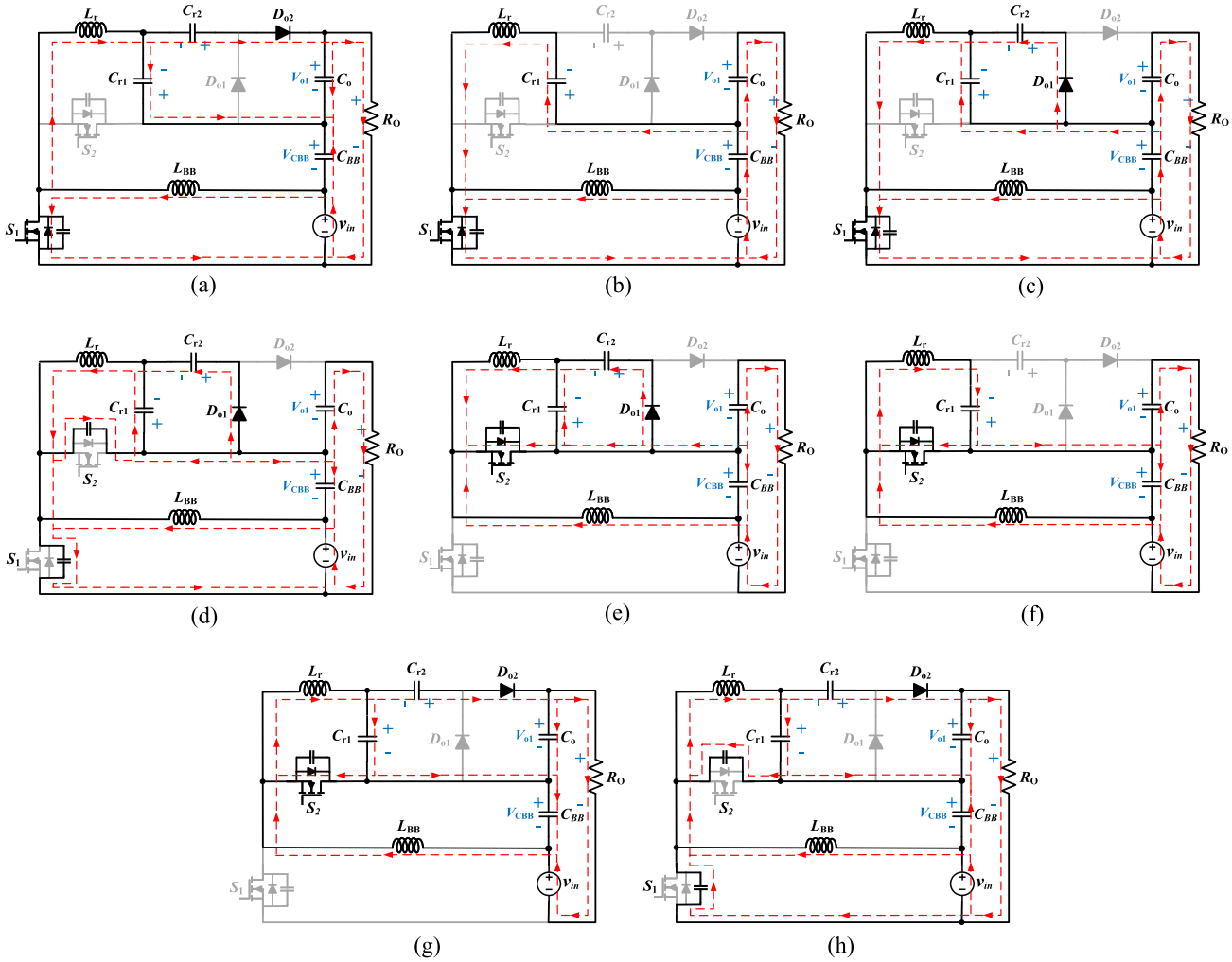

Fig. 3. Proposed converter operating modes: (a) mode 1$[t_0 - t_1]$, (b) mode 2$[t_1 - t_2]$, (c) mode 3$[t_2 - t_3]$, (d) mode 4$[t_3 - t_4]$, (e) mode 5$[t_4 - t_5]$, (f) mode 6$[t_5 - t_6]$, (g) mode 7$[t_6 - t_7]$, and (h) mode 8$[t_7 - t_8]$.

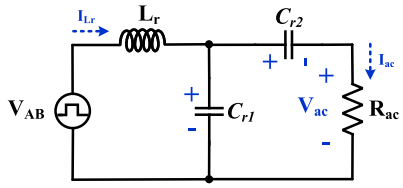

Fig. 4. *LCC* resonant network ac equivalent circuit.

where I_{Lr} and I_{LBB} are the resonant inductor current and the average buck–boost inductance current, respectively, and are calculated as follows:

$$I_{LBB} = I_{\text{in}} = \frac{P_o}{V_{\text{in}}} \tag{9}$$

$$I_{Lr} = \frac{2V_{\text{in}}\sin(\pi D)}{\pi(1-D)Z_0}\sqrt{\frac{1}{Q^2} + \frac{(1+C_n)^2}{C_n^2}}\cos(\omega_s t - \theta) \tag{10}$$

$$\theta = \tan^{-1}\left(Q\left(\frac{1+C_n}{C_n}\right)\right). \tag{11}$$

The output diodes voltage stress ($V_{D,\text{peak}}$), current stress ($I_{D,\text{peak}}$), and the average current ($I_{D,\text{avg}}$) are equal to V_o, (πI_o), and I_o, respectively.

The proposed converter switches and diodes voltage stress versus the duty cycle are shown in Fig. 6(a). According to this figure, at duty cycles close to 0.5, the switches voltage stress is at its minimum value, while the diodes voltage stress is at maximum.

According to the aforementioned analysis of the semiconductor elements voltage and current stresses, appropriate switches and diodes can be selected.

C. Soft-Switching Condition

In the proposed converter, both currents I_{LBB} and I_{Lr} flow through the main switches. Therefore, the effect of both of these currents should be considered in investigating the ZVS condition. At t_3, I_{Lr} is positive (and I_{LBB} is always positive), so (-(I_{Lr}+I_{LBB})) current is negative at S_2 turn-ON instant and provides a strong ZVS turn-ON for S_2. However, I_{Lr} is negative at t_7, and (I_{Lr}+ I_{LBB}) current is responsible for providing the S_1

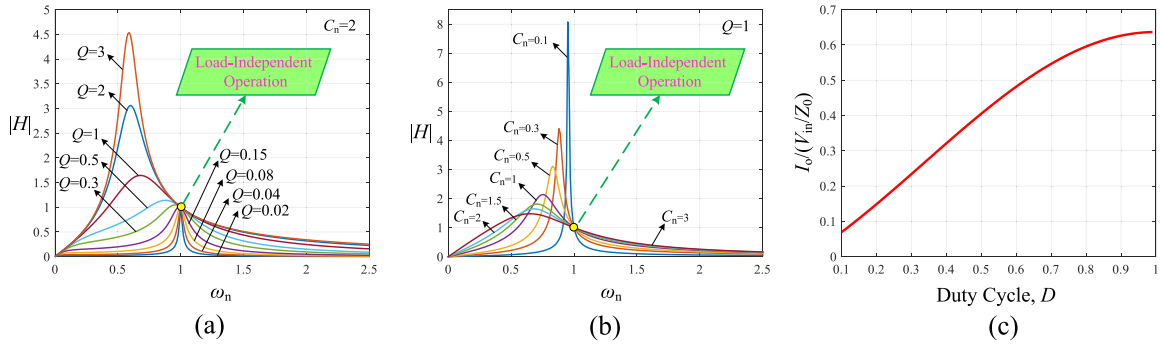

Fig. 5. Current gain graphs. (a) *LCC* resonant network at different quality factors. (b) *LCC* resonant network at different resonant capacitors ratios. (c) Normalized output current.

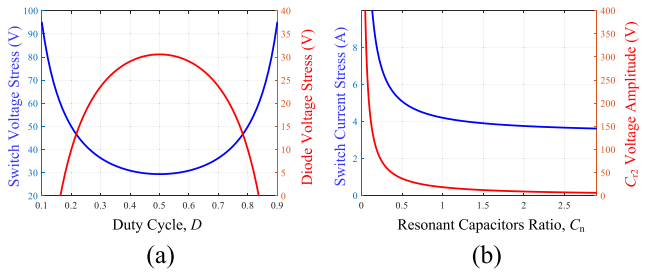

Fig. 6. (a) Switch and diode voltage and current stress at various duty cycles. (b) Switch current stress and C_{r2} voltage versus C_n.

ZVS turn-ON condition. Therefore, the ZVS turn-ON condition is more critical for S_1; as a result, if the ZVS turn-ON condition is provided for S_1, it would also be provided for S_2. To ensure S_1 ZVS turn-ON condition, condition (12) must be satisfied for the entire input voltage and operating duty cycles.

$$-(I_{Lr}(t_7) + I_{LBB}(t_7)) \geqslant \frac{C_{oss} V_{S1,\text{peak}}}{t_d} \tag{12}$$

where C_{oss} is the switch output capacitor and t_d is the deadtime between the switches gate signals.

IV. Experimental Result

To verify the proposed converter performance, a 21-W laboratory prototype operating at 200 kHz switching frequency is realized and tested for the wide input voltage range of 12–40 V and 350 mA output current.

The characteristic impedance $Z_0 = 17\ \Omega$ is obtained using (7). By obtaining the Z_0 value, the values of $L_r = 13.6\ \mu H$ and 46.9 nF are calculated from the following relations:

$$L_r = \frac{Z_0}{2\pi f_r} \quad , \quad C_{r1} = \frac{1}{2\pi f_r Z_0}. \tag{13}$$

The resonant capacitors ratio $C_n \leq 2$ is necessary for satisfying the soft-switching condition set by (12). However, as shown in Fig. 6(b), the switches current stress and C_{r2} voltage amplitude increase with decreasing C_n. Therefore, $C_n = 2$ is chosen to provide the switches ZVS turn-ON condition while preventing increased conduction loss and C_{r2} voltage amplitude. By determining the C_n and C_{r1} values, $C_{r2} = 93.8$ nF is calculated as $C_{r2} = C_{r1}\ C_n$. Designing L_m is just like the conventional buck–boost converter for current ripple below 10% as follows:

$$L_m = \frac{V_{\text{in}} D}{0.1 I_{LBB} f_s} \geqslant 200\,\mu H. \tag{14}$$

The proposed converter prototype specifications are given in Table I, and the picture of the implemented converter prototype is shown in Fig. 7. According to the prototype circuit, EE 22-19 ferrite core with PC44 material is employed for the resonant inductor. Also, high-quality low ESR MKT capacitors are used for the resonant capacitors (C_{r1} and C_{r2}). The diodes and switches experimental current and voltage waveforms for 12 and 40 V input voltages are presented in Figs. 8 and 9, respectively.

TABLE I
Prototype Parameters and Components

Parameter/Component	Specification
DC Input Voltage, V_{in}	12-40 V
Output Current, I_o	0.35 A
Output Power, P_o	21 W
Switching Frequency, f_s	200 kHz
Resonant Inductor, L_r	13.6 μH
Resonant Capacitor, C_{r1}	46.9 nF
Resonant Capacitor, C_{r2}	93.8 nF
Buck-Boost Inductor, L_{BB}	200 μH
Buck-Boost Capacitor, C_{BB}	22 μF
Output Capacitor, C_o	33 μF
Main switches, S_1, S_2	IPP075N15N3G
Sedondary Diodes, D_{o1}, D_{o2}	SB560L

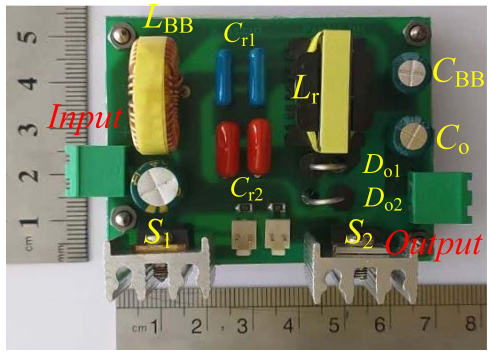

Fig. 7. Implemented converter prototype.

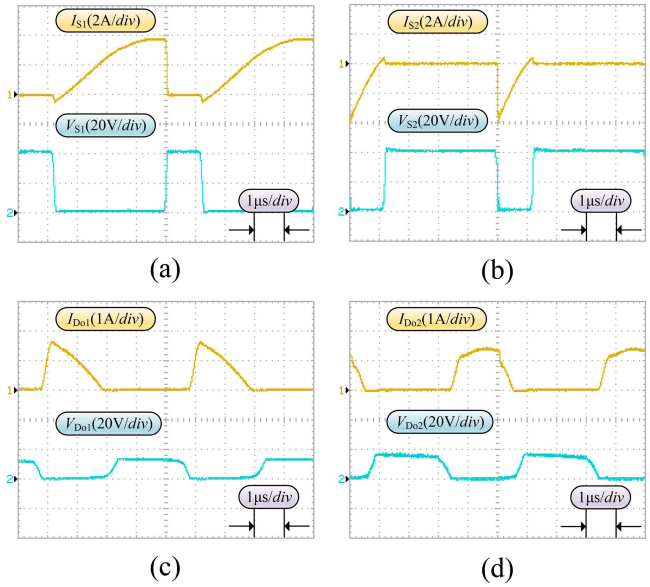

Fig. 8. Experimental voltage and current waveforms for 12-V input voltage. (a) S_1. (b) S_2. (c) D_{o1}. (d) D_{o2}.

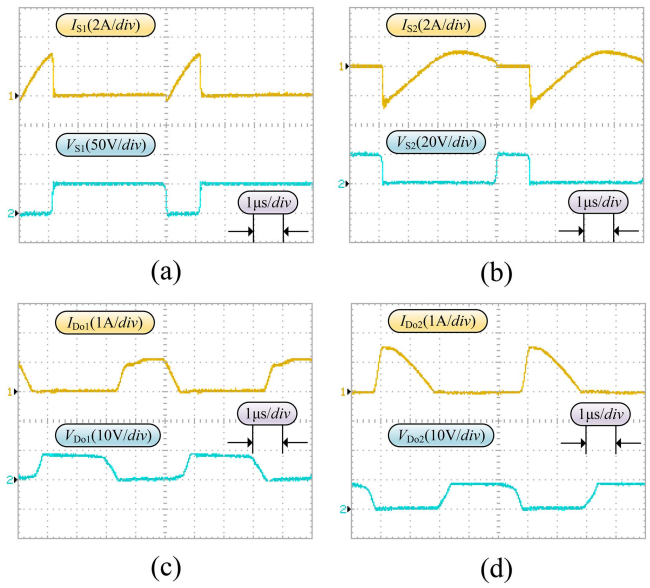

Fig. 9. Experimental voltage and current waveforms for 40-V input voltage. (a) S_1. (b) S_2. (c) D_{o1}. (d) D_{o2}.

As observed, the switches ZVS turn-ON and diodes ZCS turn-OFF condition for the entire input voltage range is maintained, which causes limited switching and reverse recovery losses, respectively. The resonant network elements waveforms for high and low input voltages are shown in Fig. 10. In Fig. 11 the dynamic response of the proposed converter with abrupt input voltage changes from 12 to 40 V and vice versa is shown. Similar to the method presented in [4] and [20], in the experiment, an additional small inductor of 10 μH is used in series with the LED load to reduce the current surges during the input voltage transitions. The proposed converter detailed loss breakdown

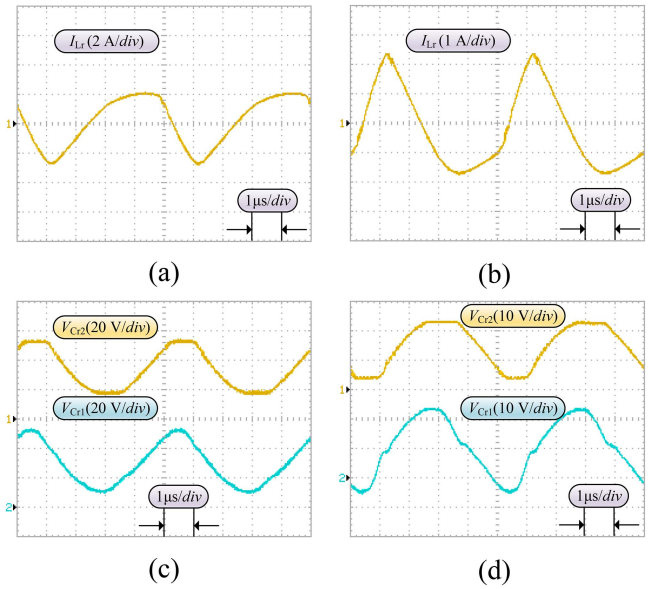

Fig. 10. Experimental waveforms of: (a) I_{Lr} at 12 V, (b) I_{Lr} at 40 V, (c) V_{Cr1} and V_{Cr2} at 12 V, and (d) V_{Cr1} and V_{Cr2} at 40 V.

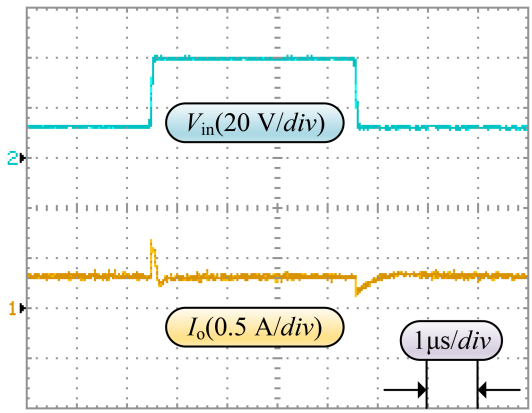

Fig. 11. Dynamic response of the proposed converter with input voltage changes from 12 to 40 V and vice versa.

analysis at $V_{in} = 12$ V and $V_{in} = 40$ V are shown in Fig. 12, and the efficiency versus input voltage is illustrated in Fig. 13. As shown, the highest efficiency of the proposed converter is about 98.15%. This high efficiency of the proposed converter comes from the ZVS switched structure, and the output power is delivered through no-processed paths and also operating at the resonance frequency. The proposed converter is compared with some nonisolated load-independent wide-input ZVS soft-switched fixed-frequency resonant converters in Table II. As observed, the proposed converter has a lower component number than [1] and [20] and same component number with [4]. Also, the proposed converter efficiency is much higher than other counterparts. In addition, the proposed converter has lower circuit complexity in comparison with [1] and [20], which use six and four power switches, respectively. It should be noted that the converter presented in [1] suffers from circulating current due to its phase-shifted control.

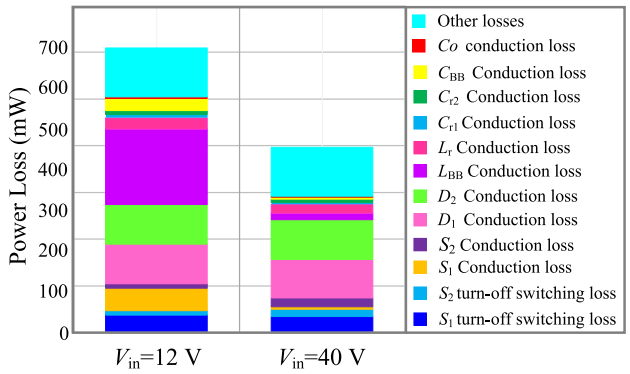

Fig. 12. Power loss distribution at minimum and maximum input voltages and full-load condition.

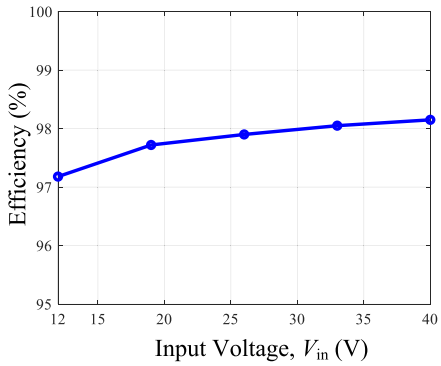

Fig. 13. Proposed converter efficiency versus input voltage.

TABLE II
COMPARISON OF WIDE INPUT STATE OF THE ART ISOLATED CONVERTERS

Topologies	[4]	[20]	[1]	Proposed Converter
Switches	2	4	6	2
Diodes	2	4	-	2
Capacitors	2	2	2	2
Inductors	2	2	3	2
Magnetic Cores	2	2	3	2
Resonant Tank Type	LCC	LC	LCL	LCC
Operation	PWM	PWM	PSC *	PWM
Maximum Efficiency (%)	95.8	94.1	87.5	98.15
Rated Power (W)	40	22.77	20	21

*. Phase Shifted Control

V. CONCLUSION

A novel highly efficient nonisolated constant output current resonant converter with low element count for wide input voltage range applications is proposed in this article. A buck–boost is combined with an *LCC* resonant converter to increase the wide voltage conversion ratio range. Also, the input voltage source and the buck–boost output are connected in series with the voltage-doubler rectifier output to improve the efficiency by decreasing the processed power. This such topology also brings other advantages, such as wide adjustable voltage gain and low inverter switches, and output rectifier diodes voltage stress. The load-independent output current specification is achieved by operating the *LCC* network at resonant frequency. All proposed converter switches and diodes operate at soft switching within a wide range of the input voltages and load conditions. The results are obtained from a converter laboratory prototype with a wide input voltage range of 12–40 V and 0.35 A constant output current, which is regulated by a fixed-frequency PWM control scheme that validates the converter theoretical analysis. The proposed converter achieves a high peak efficiency of 98.15%.

REFERENCES

[1] S. Mukherjee, V. Yousefzadeh, A. Sepahvand, M. Doshi, and D. Maksimović, "High-frequency wide-range resonant converter operating as an automotive LED driver," *IEEE Trans. Emerg. Sel. Topics Power Electron.*, vol. 9, no. 5, pp. 5781–5794, Oct. 2020.

[2] F. Pouladi, H. Farzanehfard, E. Adib, and H. Le Sage, "Single-switch soft-switching LED driver suitable for battery-operated systems," *IEEE Trans. Ind. Electron.*, vol. 66, no. 4, pp. 2726–2734, Apr. 2019.

[3] Y. Yuan, L. Lai, and Q. Wu, "A current-fed LCL resonant converter for wide output-voltage applications," *IEEE Trans. Ind. Electron.*, vol. 68, no. 5, pp. 3939–3948, May 2020.

[4] N. Molavi and H. Farzanehfard, "Load-independent hybrid resonant converter for automotive LED driver applications," *IEEE Trans. Power Electron.*, vol. 37, no. 7, pp. 8199–8206, Jul. 2022.

[5] J. Xu, Y. Sun, G. Xu, X. Liang, and M. Su, "Current-fed LC series resonant converter with load-independent voltage-gain characteristics for wide voltage range applications," *IEEE Trans. Power Electron.*, vol. 36, no. 10, pp. 11509–11522, Oct. 2021.

[6] N. D. Dao et al., "High-efficiency hybrid LLC resonant converter for on-board chargers of plug-in electric vehicles," *IEEE Trans. Power Electron.*, vol. 35, no. 8, pp. 8324–8334, Aug. 2020.

[7] L. Gu, X. Zhang, and P. Li, "Hybrid-PWM-controlled current-fed bidirectional series resonant converter with low current ripple and wide voltage gain," *IEEE Trans. Ind. Electron.*, vol. 68, no. 8, pp. 7125–7136, Aug. 2021.

[8] J.-W. Lim, J. Hassan, and M. Kim, "Bidirectional soft switching push–pull resonant converter over wide range of battery voltages," *IEEE Trans. Power Electron.*, vol. 36, no. 11, pp. 12251–12267, Nov. 2021.

[9] Y. Wei, Q. Luo, and H. A. Mantooth, "An LLC converter with multiple operation modes for wide voltage gain range application," *IEEE Trans. Ind. Electron.*, vol. 68, no. 11, pp. 11111–11124, Nov. 2021.

[10] J. Wu, X. Yan, X. Sun, X. Su, H. Du, and X. Wang, "A series resonant three-port DC–DC converter with decoupling function and magnetic integration," *IEEE Trans. Power Electron.*, vol. 37, no. 12, pp. 14720–14737, Dec. 2022.

[11] Y. Xuan, X. Yang, W. Chen, T. Liu, and X. Hao, "A novel three-level CLLC resonant DC–DC converter for bidirectional EV charger in DC microgrids," *IEEE Trans. Ind. Electron.*, vol. 68, no. 3, pp. 2334–2344, Mar. 2021.

[12] Y. Zuo, X. Pan, and C. Wang, "A reconfigurable bidirectional isolated LLC resonant converter for ultra-wide voltage-gain range applications," *IEEE Trans. Ind. Electron.*, vol. 69, no. 6, pp. 5713–5723, Jun. 2022.

[13] J.-W. Kim and P. Barbosa, "PWM-controlled series resonant converter for universal electric vehicle charger," *IEEE Trans. Power Electron.*, vol. 36, no. 12, pp. 13578–13588, Dec. 2021.

[14] Y. Shen, H. Wang, A. Al-Durra, Z. Qin, and F. Blaabjerg, "A structure-reconfigurable series resonant DC–DC converter with wide-input and configurable-output voltages," *IEEE Trans. Ind. Appl.*, vol. 55, no. 2, pp. 1752–1764, Mar./Apr. 2019.

[15] Y. Shen, H. Wang, Z. Shen, Y. Yang, and F. Blaabjerg, "A1-MHz series resonant DC–DC converter with a dual-mode rectifier for PV microinverters," *IEEE Trans. Power Electron.*, vol. 34, no. 7, pp. 6544–6564, Jul. 2019.

[16] W. Sun, Y. Xing, H. Wu, and J. Ding, "Modified high-efficiency LLC converters with two split resonant branches for wide input-voltage range applications," *IEEE Trans. Power Electron.*, vol. 33, no. 9, pp. 7867–7879, Sep. 2018.

[17] Y. Jeong, J.-K. Kim, J.-B. Lee, and G.-W. Moon, "An asymmetric half-bridge resonant converter having a reduced conduction loss for DC/DC power applications with a wide range of low input voltage," *IEEE Trans. Power Electron.*, vol. 32, no. 10, pp. 7795–7804, Oct. 2016.

[18] Y. Yuan, L. Lai, Q. Wu, and C. Yi, "An integrated boost-LC-resonant-flyback multimode converter for battery charger applications," *IEEE Trans. Ind. Electron.*, vol. 68, no. 12, pp. 12196–12205, Dec. 2021.
[19] J. Kim, S.-W. Ryu, M. Kim, and J.-W. Jung, "Triple-mode isolated resonant buck–boost converter over wide input voltage range for residential applications," *IEEE Trans. Ind. Electron.*, vol. 68, no. 11, pp. 11087–11099, Nov. 2020.
[20] V. S. Veeramallu, S. Porpandiselvi, and B. Narasimharaju, "A nonisolated wide input series resonant converter for automotive LED lighting system," *IEEE Trans. Power Electron.*, vol. 36, no. 5, pp. 5686–5699, May 2021.

Shirin Askari was born in Iran in 1991. She received the M.Sc. degree in electrical engineering from the Shahid Bahonar University of Kerman, Kerman, Iran, in 2018. Since September 2020, she has been working toward the Ph.D. degree in electrical engineering with the Isfahan University of Technology, Isfahan, Iran.

Her current research interests include power electronics systems, high-frequency soft-switching converters, resonant converters, fixed-frequency wide range resonant converters, LED drivers, and battery chargers.

Hosein Farzanehfard (Member, IEEE) was born in Isfahan, Iran, in 1961. He received the B.Sc. and M.Sc. degrees from the University of Missouri, Columbia, MO, USA, in 1983 and 1985, respectively, and the Ph.D. degree from Virginia Polytechnic Institute and State University, Blacksburg, VA, USA, in 1992, all in electrical engineering.

Since 1993, he has been a Faculty Member with the Department of Electrical and Computer Engineering, Isfahan University of Technology, Isfahan, Iran. He has authored/coauthored of more than 250 technical papers published in journals and conference proceedings. His current research interests include high-frequency soft-switching converters, power factor correction, bidirectional converters, active power filters, high-frequency electronic ballasts, and pulse power applications.